JOURNAL OF COMPUTATIONAL PHYSICS 62, 199–220 (1986)

An Algorithm for the Simulation of Transient Viscoelastic Flows with Free Surfaces

ROLAND KEUNINGS

Miller Institute for Basic Research in Science,
Department of Chemical Engineering, and,
Lawrence Berkeley Laboratory, University of California,
Berkeley, California 94720

Received October 16, 1984; revised February 20, 1985

We propose a numerical procedure for solving a class of transient viscoelastic flows with free surfaces. It is based on a Galerkin/Finite Element technique on deforming elements combined with a predictor-corrector scheme. The method is applied to the analysis of jet breakup caused by capillary forces. Non-linear effects known to experimentalists are predicted and a detailed comparison with asymptotic results is carried out.

INTRODUCTION

It is well established that the range of validity of the Newtonian constitutive model is limited to low molecular weight fluids. The surprising phenomena associated with the flow of polymeric materials cannot be explained on the basis of the Navier–Stokes equations. Non-Newtonian behavior has many facets. Among them are the presence of normal stresses in viscometric flows, the shear-rate dependence of the shear viscosity, high resistance to elongational deformation, and memory effects associated with the elasticity of the material. A large number of constitutive models have been developed (and indeed are still being developed) to describe non-Newtonian behavior (see, e.g., Bird *et al.* [1]), but none is known to be applicable in all flow situations. This is in marked contrast to Newtonian fluid mechanics, where one does not question the very form of the mathematical problem to be solved.

In this context, the numerical simulation of the flow of highly elastic liquids in complex geometries has attracted the attention of many research groups. Two comprehensive reviews on this subject are available (Crochet and Walters [11], Crochet *et al.* [6]). Most of the work has concentrated on steady flows, and, for reasons of tractability, simple constitutive models have been used. Examples of these are the Maxwell and Oldroyd-B fluids; they constitute valid formulations for arbitrary large deformations of the material, and can, at least qualitatively, account for many of the observed elastic effects. Most applications involving polymer liquids occur at low or negligible Reynolds numbers. The numerical solution of viscoelastic

0021-9991/86 $3.00

flows has proven very difficult, however, in view of the non-linearities present in the constitutive models. Although considerable success has been achieved in the last few years, obtaining reliable solutions at high elasticity remains a challenge.

There are strong motivations to develop numerical techniques for solving transient viscoelastic flows. One is of course the large number of interesting applications. Another stems from the difficulties encountered by steady algorithms in obtaining results for high elasticity; a transient approach might reveal the lack of a steady solution and generate time-periodic solutions, for example. Also of relevance is the application of a transient scheme to the non-linear analysis of the stability of viscoelastic flows.

Few numerical solutions of transient viscoelastic flows in complex geometries have been described in the literature, probably because of the enormous amount of computer resources involved. Indeed, only four papers dealing with the subject have been published as of this writing, and no solution of a flow problem with a free surface has ever been reported. Hassager and Bisgaard [19] have proposed a Lagrangian finite element technique based on a variational formulation of the flow of a Maxwell fluid (Hassager [18]); they have applied their method to the problem of a sphere suddenly set in motion in a cylinder containing an initially quiescent fluid. Lee *et al.* [26] have studied the slow compressive flow of a Maxwell fluid between two parallel disks. Here, the constitutive model is written in its differential form, and Lagrangian coordinates are used to simplify the formulation. Spatial discretization is achieved by means of the mixed finite element technique developed by Crochet and Keunings [7], and a predictor–corrector scheme is used to determine the nodal motion. These two Lagrangian techniques are well suited for flow problems involving small deformations of the grid; they become much less feasible, however, when large deformations take place, which is the case in various free surface problems and in a majority of flows in confined geometries.

Two reports have appeared of the solution of transient viscoelastic flow equations in Eulerian form. Finlayson [12] has studied the stability of fully developed flows in a circular pipe by means of a Petrov/Galerkin method for spatial discretization, combined with a first-order time integrator. The constitutive models used in his work are direct generalizations of the Maxwell model, allowing for viscosities and relaxation times dependent of the rate of deformation. A finite difference method has also been proposed recently by Townsend [35] for solving the flow of an Oldroyd–B fluid past a circular cylinder. Here, a smoothing procedure is used to stabilize the time integration for high elasticity numbers; as a result, this method is more a pseudo-transient algorithm for obtaining steady solutions than a true transient scheme.

In this paper, we present an algorithm for solving a class of transient viscoelastic flows with free surfaces. It is based on a Galerkin/Finite Element method on deforming elements combined with a predictor–corrector scheme for the temporal integration. Numerical methods using deforming finite element grids have been developed in the last few years for solving a broad range of moving boundary problems (Lynch [28]). In the context of Newtonian fluid mechanics, for example,

Frederiksen and Watts [13] have applied the space-time finite element method of Bonnerot and Jamet [3], while Kheshgi and Scriven [25] have suggested a Galerkin technique combined with a penalty treatment of the incompressibility constraint. A conceptual framework common to these different techniques has been established by Lynch [28]; it is adopted in the present paper, and its main features can be described as follows: the unknown fields are interpolated by finite element basis functions defined on a continuously deforming grid; the displacement of the free surface is unknown a priori and is determined simultaneously with the unknown fields; at each discrete time step, the grid is deformed to follow the motion of the free boundary in a way that avoids excessive element deformation; this grid motion is properly accounted for in the formulation of the discretized problem.

For the sake of illustration, we consider the flow of an Oldroyd–B fluid; extension to more complex models such as those used in recent steady simulations (Keunings *et al.* [22]; Keunings and Crochet [23]) does not present any significant difficulty. In addition, we assume that the free surface can be represented by a height function. Here also, other representations for the free boundary can be envisaged to handle more complex situations (Hirt and Nichols [20]; Kheshgi and Scriven [25]). The method has been implemented for two-dimensional plane or axisymmetric geometries (with or without a free surface); solving three-dimensional problems does not involve new principles, but is simply out of the question for obvious practical reasons.

We apply the numerical technique to the simulation of capillary instabilities leading to the breakup of liquid jets into droplets. This problem arises in many applications, including ink-jet printing technology, new techniques for measuring elongational properties of polymeric solutions, and various atomization processes (Schummer and Tebel [34]). Theoretical investigations of Newtonian jets in the laminar regime have achieved a considerable success in predicting observed phenomena (McCarthy and Molloy [30]; Bogy [2]), but such is not the case with viscoelastic jets. Experimental work with polymeric solutions has revealed the remarkable stabilizing effect of elastic forces on the breakup process; indeed, viscoelastic jets generally take longer to disintegrate into droplets than Newtonian jets of comparable shear viscosity (see, e.g., Gordon *et al.* [15]). The theoretical studies aimed at explaining this behavior have been based on linear stability analyses. In this context, one considers the growth of infinitesimal disturbances applied to a fully relaxed jet and leading to breakup; the governing equations are linearized, as well as the boundary conditions which are applied at the unperturbed jet surface. Since the deformations are assumed to be small, the rheological behavior of the fluid is unambiguously described by the general linear viscoelastic model (Christensen [5]). The results indicate a destabilizing effect of elastic forces, which appears to be in disagreement with experimental evidence and suggests that the breakup process is dominated by non-linear effects (Middleman [31]; Goldin *et al.* [16]). Two complementary non-linear analyses of viscoelastic jet breakup have been carried out recently; one is based on a unidimensional model of the jet

dynamics, while the other consists of the numerical simulation of the full two-dimensional flow by means of the method presented in this paper. Preliminary results have been reported by Bousfield *et al.* [4] for the one-dimensional analysis, and by the present author (Keunings [24]) for the numerical study. Both approaches are able to predict the stabilizing nature of elasticity, and show that it results from non-linear behavior associated with the buildup of elongational stresses during the growth of the disturbances.

In the present paper, we focus on a detailed comparison between numerical and linearized analytical results. The latter are asymptotically valid for small deformations of the jet surface, and thus provide a relevant check of the accuracy of the numerical procedure. In order to achieve a meaningful comparison, we study the growth of a small cosinusoidal perturbation initially applied to the radius of a cylindrical jet, and we select as initial conditions for the flow field the linearized analytical solution corresponding to the applied perturbation. The analytical solution is based on the linear theory proposed by Middleman [31] for the Oldroyd–B model. It is found that the numerical results for both Newtonian and Oldroyd–B fluids are in excellent agreement with the analytical predictions at the beginning of the growth. At later times, the numerical analysis predicts a non-cosinusoidal deformation of the jet surface due to non-linear effects. This leads in the Newtonian case to the birth of satellite drops; in the viscoelastic case, a pattern of drops connected by slowly stretched filaments is achieved. Both phenomena have been observed experimentally (Bogy [2]; Gordon *et al.* [15]); they cannot be predicted by the linear theory, which is shown here to be increasingly inaccurate when finite deformations of the jet surface take place.

Governing Equations

The isothermal flow of a viscoelastic fluid is governed by a set of conservation and constitutive equations. The former express the principles of conservation of mass and momentum, while the latter describe the rheological behavior of the specific class of materials under consideration. These equations are typically written in terms of three unknown fields: the velocity field $\mathbf{v}$, the pressure field p, and the extra-stress field $\mathbf{T}$. The latter is related to the Cauchy stress tensor $\boldsymbol{\sigma}$ through

$$\boldsymbol{\sigma} = -p\mathbf{I} + \mathbf{T}, \tag{1}$$

where $\mathbf{I}$ is the unit tensor. In general, the unknown fields depend on time t and the set of independent space variables $\mathbf{x}$. Compressibility effects can be neglected in most applications so that the mass conservation equation reduces to the kinematic constraint

$$\nabla \cdot \mathbf{v} = 0. \tag{2}$$

The momentum equation takes the familiar form

$$\rho \frac{D\mathbf{v}}{Dt} = -\nabla p + \nabla \cdot \mathbf{T} + \mathbf{f}, \tag{3}$$

where ρ denotes the density, D/Dt is the material derivative, i.e.,

$$\frac{D\mathbf{v}}{Dt} = \frac{\partial \mathbf{v}}{\partial t} + \mathbf{v} \cdot \nabla \mathbf{v}, \tag{4}$$

and $\mathbf{f}$ is the body force per unit volume. Closure is obtained with a constitutive model relating the extra-stress field to the deformation experienced by the material. In this paper, we consider the flow of an Oldroyd–B fluid (Oldroyd [32]) whose rheological behavior is defined by

$$\mathbf{T} + \lambda_1 \overset{\nabla}{\mathbf{T}} = 2\mu[\mathbf{D} + \lambda_2 \overset{\nabla}{\mathbf{D}}]. \tag{5}$$

Here, the symbol $\overset{\nabla}{\mathbf{T}}$ stands for the upper-convected derivative of $\mathbf{T}$ defined as

$$\overset{\nabla}{\mathbf{T}} = \frac{D\mathbf{T}}{Dt} - (\nabla \mathbf{v})^T \cdot \mathbf{T} - \mathbf{T} \cdot \nabla \mathbf{v}, \tag{6}$$

while $\mathbf{D}$ is the rate of strain tensor, $\frac{1}{2}(\nabla \mathbf{v} + \nabla \mathbf{v}^T)$. The Oldroyd–B model contains three material constants (a shear viscosity μ, a relaxation time λ_1 and a retardation time λ_2) which are determined from appropriate rheometrical experiments (Walters [36]). Despite its relative simplicity, the Oldroyd–B model is known to be adequate to describe the rheology of some polymer solutions (see, e.g., Jackson *et al.* [21]).

Inspection of equations (5–6) reveals the implicit character of the stress–strain relationship. This prevents the direct elimination of $\mathbf{T}$ in the momentum equation (3) and requires the use of a mixed numerical technique in which extra-stresses, together with velocities and pressure, are basic unknowns. Another difficulty comes from the presence in (5) of the term $\overset{\nabla}{\mathbf{D}}$. It contains second-order spatial derivatives of the velocity field, the presence of which is computationally inconvenient. We can, however, rewrite (5) in the following manner:

$$\mathbf{T} = \mathbf{T}_1 + \mathbf{T}_2, \tag{7}$$

$$\mathbf{T}_1 + \lambda_1 \overset{\nabla}{\mathbf{T}}_1 = 2\mu_1 \mathbf{D}, \tag{8}$$

$$\mathbf{T}_2 = 2\mu_2 \mathbf{D}. \tag{9}$$

Equivalence of the two formulations is obtained if

$$\mu = \mu_1 + \mu_2, \qquad \lambda_2 = \lambda_1 \mu_2 / \mu \tag{10}$$

(Crochet and Keunings [9]). We shall refer to $\mathbf{T}_1$ and $\mathbf{T}_2$ as the elastic and Newtonian components of the extra-stress tensor, respectively.

Upon elimination of $\mathbf{T}_2$ in the momentum equation (3), we obtain the set of nonlinear partial differential equations

$$\mathbf{T}_1 + \lambda_1 \overset{\nabla}{\mathbf{T}}_1 = 2\mu_1 \mathbf{D}, \tag{11}$$

$$\rho \frac{D\mathbf{v}}{Dt} = -\nabla p + 2\mu_2 \nabla \cdot \mathbf{D} + \nabla \cdot \mathbf{T}_1 + \mathbf{f}, \tag{12}$$

$$\nabla \cdot \mathbf{v} = 0, \tag{13}$$

to be solved in terms of $\mathbf{T}_1$, $\mathbf{v}$ and p in a flow domain Ω. In the presence of a free surface, the flow domain is an unknown function of time $\Omega(t)$. We will assume that Ω is two-dimensional (either planar or axisymmetric), and that the free surface, if any, can be represented by a function of time and a single space coordinate (see Fig. 1). In that case, the evolution of the deforming flow domain can be determined through the kinematic condition

$$\frac{\partial h}{\partial t} + v_x \frac{\partial h}{\partial x} = v_y, \tag{14}$$

where v_x and v_y are the velocity components at the free surface. The unknown function h will be referred to as the height function.

Initial and boundary conditions relevant to a specific problem must also be supplied. We prescribe initial values for the velocity and the elastic part of the stress. Boundary conditions may include the specification of the velocity components or the contact force on part of the boundary $\partial\Omega$; values of the elastic stress are imposed at an entry section, and a reference pressure must be defined at one point of the flow domain if no surface force condition is imposed. At a free surface (that is, a liquid–gas interface) continuity of stress leads to the condition

$$\boldsymbol{\sigma} \cdot \mathbf{n} = -p_g \mathbf{n} + \gamma \left(\frac{1}{R_1} + \frac{1}{R_2} \right) \mathbf{n}, \tag{15}$$

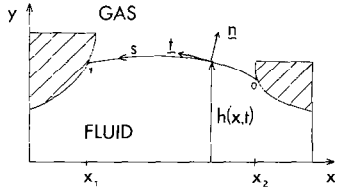

Fig. 1. A typical flow domain with a free surface represented by the height function h.

where $\mathbf{n}$ is the unit normal to the free surface, p_g is the ambient gas pressure, γ is the coefficient of surface tension and R_1, R_2 are the principal radii of curvature of the interface (Levich [27]). The latter are directly related to the height function and its derivatives. For example, assuming that the flow domain depicted in Fig. 1 is axisymmetric around the x-axis, one has

$$R_1 = \left[1 + \left(\frac{\partial h}{\partial x}\right)^2\right]^{3/2} \Big/ \frac{\partial^2 h}{\partial x^2}, \tag{16}$$

$$R_2 = -h\left[1 + \left(\frac{\partial h}{\partial x}\right)^2\right]^{1/2}. \tag{17}$$

For plane flows, the expression for R_1 remains valid, while R_2 becomes infinite. Finally, we complete the mathematical formulation with initial and boundary conditions for the height function.

Numerical Technique

The numerical technique is based on a Galerkin/Finite Element discretization of the governing equations combined with a finite difference scheme for the integration in time. Simply stated, the algorithm goes as follows: the simulation starts marching forward in time from given initial data and an initial finite element mesh. At each time step, the flow field and the location of the free surface are determined by means of a predictor–corrector scheme. The grid deforms during the simulation to follow the displacement of the free surface, and internal nodes are moved such as to preserve the initial topology of the element layout. This nodal motion is anchored to the displacement of the free surface and is appropriately accounted for in the Galerkin formulation.

More precisely, let us define approximations of the finite element type for the elastic part of the extra-stress, the velocity, and the pressure as follows:

$$\mathbf{T}_1^*(\mathbf{x}, t) = \sum_i \mathbf{T}_1^i(t)\phi_i, \qquad \mathbf{v}^*(\mathbf{x}, t) = \sum_j \mathbf{v}^j(t)\psi_j, \qquad p^*(\mathbf{x}, t) = \sum_k p^k(t)\pi_k. \tag{18}$$

In these expressions, the symbols ϕ_i, ψ_j, and π_k represent given finite element basis functions, while $\mathbf{T}_1^i$, $\mathbf{v}^j$, and p^k are unknown time-dependent nodal values. The basis functions depend only on position when a fixed grid is used. If nodal motion is allowed, they become implicit functions of time through the location of the nodes; one has, for example, that

$$\phi_i = \phi_i(\mathbf{x}, \mathbf{X}_m(t)), \tag{19}$$

where the $\mathbf{X}_m$ are nodal position vectors.

We invoke the Galerkin principle to discretize (11–13) in space. This requires that residuals obtained after substitution of (18) in (11–13) be orthogonal to the set of basis functions, giving

$$\int_{\Omega(t)} \phi_i [\mathbf{T}_1^* + \lambda_1 \overset{\nabla}{\mathbf{T}}_1^* - 2\mu_1 \mathbf{D}^*] \, d\Omega = \mathbf{0}, \tag{20}$$

$$\int_{\Omega(t)} \left\{ \psi_j \left[\rho \frac{D\mathbf{v}^*}{Dt} - \mathbf{f} \right] + \nabla \psi_j^T \cdot [-p^* \mathbf{I} + 2\mu_2 \mathbf{D}^* + \mathbf{T}_1^*] \right\} d\Omega = \int_{\partial\Omega(t)} \psi_j \boldsymbol{\sigma}^* \cdot \mathbf{n} \, d\partial\Omega, \tag{21}$$

$$\int_{\Omega(t)} \pi_k [\nabla \cdot \mathbf{v}^*] \, d\Omega = 0. \tag{22}$$

Here, every term marked by an asterisk denotes the corresponding finite element approximation obtained from (18). For the sake of brevity, we have written the Galerkin principle in a closed form valid for cartesian tensors in an orthogonal coordinate system. When dealing with an axisymmetric flow domain, we use the proper formulation derived in a cylindrical coordinate system. (See Crochet *et al.* [6] for details in the particular case of steady flows.)

In the next section, we present results obtained for both an Oldroyd–B fluid and a Newtonian fluid. The mixed technique defined by (20–22) is of course applicable in the Newtonian case where $\lambda_1 = 0$. Previous work on steady flows has clearly shown, however, that a mixed method is not an optimal choice in this particular case, whether based on a criterion of accuracy or economy of computer resources (see, e.g., Crochet and Keunings [8]; Crochet *et al.* [6]). For solving the flow of a Newtonian fluid, we use here the classical velocity–pressure Galerkin formulation of the Navier–Stokes equations which can be formally obtained from (20–22) with the selection of parameters

$$\lambda_1 = \mu_1 = 0, \qquad \mu_2 = \mu. \tag{23}$$

Equation (20) then directly gives $\mathbf{T}_1^* = \mathbf{0}$ and can therefore be ignored. The algorithm to be presented hereafter thus remains valid for a Newtonian fluid, keeping in mind that only velocity and pressure nodal values enter the Galerkin formulation in this particular case.

We have used the divergence theorem in the momentum equation (21) to reduce regularity requirements on the basis functions ψ_j and to introduce natural boundary conditions in terms of the contact force at the boundary. In particular, the stress condition (15) at the free surface is specified by direct substitution in the right-hand side of (21). It is crucial to note from inspection of (16) that the discrete representation of the free surface must be of class C^1 to preserve conformity. Such a degree of regularity, however, can be avoided by an integration by parts along the free surface. The technique has been proposed by Ruschak [33] for plane flows. In

that case, the free boundary is defined as a curve in a plane. If s denotes the arc length along this curve, and $\mathbf{t}$ the unit tangent vector, we have

$$\frac{d\mathbf{t}}{ds} = \frac{1}{R_1}\mathbf{n}, \tag{24}$$

and some terms in the boundary integral can be integrated by parts to yield

$$-\int_{s_0}^{s_1} p_g \psi_j \mathbf{n}\, ds - \gamma \int_{s_0}^{s_1} \mathbf{t} \frac{d\psi_j}{ds}\, ds + \gamma[\psi_j \mathbf{t}]_{s_1} - \gamma[\psi_j \mathbf{t}]_{s_0}. \tag{25}$$

Here, the symbols 0 and 1 refer to the endpoints of the free surface (see Fig. 1). This enables the use of a representation of class C^0 for the free surface, together with a natural specification of the endpoint tangent vectors. It is possible to extend the procedure to axisymmetric flows. Here a cylindrical coordinate system is used and the free surface is described by a meridian. The boundary term now reads

$$\int_{s_0}^{s_1} \psi_j \boldsymbol{\sigma}^* \cdot \mathbf{n}\, 2\pi r\, ds. \tag{26}$$

Since the curvature of the interface can be written as

$$\frac{d\mathbf{t}}{ds} + \frac{1}{R_2}\mathbf{n}, \tag{27}$$

we can integrate by parts the term involving a second-order derivative of the boundary representation. We obtain

$$-\int_{s_0}^{s_1} p_g \psi_j \mathbf{n}\, 2\pi r\, ds + \gamma \int_{s_0}^{s_1} \frac{\psi_j}{R_2}\mathbf{n}\, 2\pi r\, ds - \gamma \int_{s_0}^{s_1} \mathbf{t} \frac{d(r\psi_j)}{ds} 2\pi\, ds$$

$$+ 2\pi\gamma[\psi_j r \mathbf{t}]_{s_1} - 2\pi\gamma[\psi_j r \mathbf{t}]_{s_0}, \tag{28}$$

and a representation of class C^0 for the interface is again admissible.

Special care must be taken in the evaluation of time derivatives when the Galerkin procedure is used on a moving grid. To illustrate this, let us focus on the term $\partial \mathbf{T}_1^*/\partial t$ present in (20). Because of (19), this term takes the form

$$\frac{\partial \mathbf{T}_1^*}{\partial t} = \sum_i \frac{d\mathbf{T}_1^i}{dt}\phi_i + \sum_i \mathbf{T}_1^i \frac{\partial \phi_i}{\partial t}. \tag{29}$$

The time derivative of the basis functions is related to the rate of deformation of the grid in a simple way (Lynch and Gray [29]). Indeed, consider the isoparametric transformation used to perform the integration over a deforming element:

$$\mathbf{x}(\xi, t) = \sum_m \mathbf{X}_m(t)\, \theta_m(\xi). \tag{30}$$

Here, the $\mathbf{X}_m$ are global nodal coordinates and θ_m denote basis functions defined on the parent element in the ξ space. Since the value of a basis function ϕ_i at a given point in the ξ space does not depend on time, one has

$$\left.\frac{d\phi_i}{dt}\right|_{\xi} = 0 = \frac{\partial \phi_i}{\partial t} + \left(\sum_m \frac{d\mathbf{X}_m}{dt}\theta_m\right)\cdot \nabla\phi_i. \tag{31}$$

The term $(\sum_m (d\mathbf{X}_m/dt)\theta_m)$ has the meaning of an elemental velocity field and will be denoted by $\mathbf{v}^e$. Going back to (29), we may write

$$\frac{\partial \mathbf{T}_1^*}{\partial t} = \sum_i \frac{d\mathbf{T}_1^i}{dt}\phi_i - \mathbf{v}^e \cdot \sum_i \mathbf{T}_1^i \nabla\phi_i. \tag{32}$$

In consequence, the material derivative present in (20) becomes

$$\frac{D\mathbf{T}_1^*}{Dt} = \sum_i \frac{d\mathbf{T}_1^i}{dt}\phi_i + (\mathbf{v}^* - \mathbf{v}^e)\cdot \nabla \mathbf{T}_1^*, \tag{33}$$

and a similar development for the time derivative of the velocity field yields

$$\frac{D\mathbf{v}^*}{Dt} = \sum_j \frac{d\mathbf{v}^j}{dt}\psi_j + (\mathbf{v}^* - \mathbf{v}^e)\cdot \nabla \mathbf{v}^*. \tag{34}$$

We recognize as special cases the conventional Galerkin method on a fixed mesh ($\mathbf{v}^e = \mathbf{0}$) and the purely Lagrangian approach where nodes are fluid particles ($\mathbf{v}^e = \mathbf{v}^*$). The latter method offers the combined advantages of a natural tracking of the free surface and a slight simplification of formulation. It often results in over-distorted grids as the simulation proceeds, however, and thus requires somewhat intricate remeshing procedures. We adopt here another approach which we find particularly attractive when the free surface can be represented by a height function. It consists in relating the motion of internal nodes to the displacement of the free surface. In this case, the elemental velocity field generally differs from the fluid velocity and must be accounted for as shown in (33–34).

We determine the motion of the free surface by solving the kinematic condition (14) in its weak Galerkin form. We define a one-dimensional finite element approximation for the height function in terms of nodal coefficients h^l and basis functions β_l:

$$h^*(x, t) = \sum_l h^l(t)\,\beta_l. \tag{35}$$

Here, the one-dimensional grid used for calculating h is obtained by projecting each free surface node on the $x-$ axis. The discretized kinematic condition reads

$$\int_{x_1}^{x_2} \beta_l \left[\frac{\partial h^*}{\partial t} + v_x^* \frac{\partial h^*}{\partial x} - v_y^*\right] dx = 0, \tag{36}$$

where x_1 and x_2 correspond to the endpoints of the domain of the height function (see Fig. 1), and v_x^*, v_y^* are the approximated velocity components evaluated at the free surface. The internal node motion remains to be defined. In the application to be discussed hereafter, we use the following simple law of motion for a node m:

$$x_m(t) = \text{constant}, \qquad y_m(t) = c_m h^*(x_m, t), \tag{37}$$

where c_m is a constant. This readily defines the relation between the elemental velocity field and the deformation of the flow domain.

We have not yet discussed the choice of interpolating subspaces. Previous work on the simulation of steady viscoelastic flows has favored the use of a C^0 representation on triangular or quadrilateral elements, with complete second-order polynomials for the elastic stress and the velocity and first-order polynomials for the pressure (see, e.g., Crochet and Keunings [10]). This leads to a very large number of degrees of freedom in all but the simplest situations. Clearly, in view of the enormous amount of computer time involved, the solution of complex transient flows calls for a less sophisticated approximation. In the present paper, we use isoparametric nine-node quadrilateral elements to discretize the flow domain. The height function is consistently interpolated by quadratic polynomials. The elastic stress and the pressure are given by bi-linear polynomials on the parent element, while the velocity is approximated by bi-quadratic polynomials. Every approximated field is thus of class C^0 and meets the regularity requirements implied by the Galerkin formulation.

Equations (20–22) and (36) lead to a set of first-order differential equations of the form

$$\mathbf{F}(\dot{\mathbf{T}}, \dot{\mathbf{V}}, \dot{\mathbf{H}}, \mathbf{T}, \mathbf{V}, \mathbf{P}, \mathbf{H}) = \mathbf{0}, \tag{38}$$

$$\mathbf{S}(\dot{\mathbf{H}}, \mathbf{H}, \mathbf{V}) = \mathbf{0}, \tag{39}$$

where $\mathbf{T}$, $\mathbf{V}$, $\mathbf{P}$ and $\mathbf{H}$ are vectors of nodal values of $\mathbf{T}_1$, $\mathbf{v}$, p and h, respectively, and the [illegible] variables $\mathbf{H}$ and $\dot{\mathbf{H}}$ appear in (38) through the boundary condition at the interface, the definition of the flow domain and its rate of deformation, as explained above. We solve (38–39) in a decoupled fashion. From the knowledge of the free surface and the flow field at a discrete value of time t_n, we predict the free surface and the stress and velocity fields at time t_{n+1}. We then solve (38) in the predicted flow domain in terms of $\mathbf{T}$, $\mathbf{V}$ and $\mathbf{P}$. Finally, we correct the free surface by solving (39) with the new velocity field. We use a first-order implicit scheme (Euler backward) for the integration in time of (38) and (39), mainly because of its well known A-stability property. More precisely, let $\mathbf{T}^n$, $\mathbf{V}^n$, $\mathbf{P}^n$ and $\mathbf{H}^n$ be the nodal vectors at time t_n. We obtain corresponding vectors at time $t_{n+1} = t_n + \Delta t_n$ after completion of the following steps:

(a) Prediction of the free surface and the stress and velocity fields by means of a first-order extrapolation. The free surface, for example, is predicted by

$$\mathbf{H}_{\text{pred}}^{n+1} = \mathbf{H}^n + \Delta t_n \dot{\mathbf{H}}^n. \tag{40}$$

The time derivatives $\dot{\mathbf{H}}^n$, $\dot{\mathbf{T}}^n$ and $\dot{\mathbf{V}}^n$ are known from the previous time step.

(b) Relocation of the internal nodes by means of (40) and the law of motion (37).

(c) Correction of the flow field by solving (38) on the predicted finite element grid. Applying the implicit Euler scheme to discretize (38) in time, we obtain a set of algebraic equations in terms of $\mathbf{T}^{n+1}$, $\mathbf{V}^{n+1}$ and $\mathbf{P}^{n+1}$:

$$\mathbf{F}_{\text{alg}}(\mathbf{T}^{n+1}, \mathbf{V}^{n+1}, \mathbf{P}^{n+1}; \mathbf{H}_{\text{pred}}^{n+1}, \dot{\mathbf{H}}_{\text{pred}}^{n+1}) = \mathbf{0}, \tag{41}$$

where the term $\dot{\mathbf{H}}_{\text{pred}}^{n+1}$ is approximated by $(\mathbf{H}_{\text{pred}}^{n+1} - \mathbf{H}_{\text{pred}}^{n})/\Delta t_n$. To obtain (41) from (38), time derivatives such as $\dot{\mathbf{T}}$ have been replaced by their first order approximation, i.e., $(\mathbf{T}^{n+1} - \mathbf{T}^n)/\Delta t_n$. In addition, volume and surface integrals present in (41) are evaluated on the predicted flow domain.

We solve (41) by the Newton–Raphson iterative technique with predicted values of $\mathbf{T}$ and $\mathbf{V}$ as first estimates (the pressure coefficients do not require initial estimates since they appear linearly in (41)). The derivation of the Newton–Raphson equations follows a tedious but straightforward procedure which will not be described here for the sake of brevity. Details are given by Crochet *et al.* [6] for the particular case of steady flows.

(d) Correction of the free surface by solving (39) with the velocity field $\mathbf{V}^{n+1}$ found in step (c). In this case, the time discretization of (39) leads to a linear algebraic set of the form

$$\mathbf{S}_{\text{alg}}(\mathbf{H}^{n+1}; \mathbf{V}^{n+1}) = \mathbf{0}. \tag{42}$$

(e) Evaluation of the time derivatives to be used in (a) at the next time step. This is conveniently done by simple inversion of the Euler rule. For example, we have

$$\dot{\mathbf{T}}^{n+1} = (\mathbf{T}^{n+1} - \mathbf{T}^n)/\Delta t_n. \tag{43}$$

The first time step requires a special treatment. We skip the prediction procedure and determine the flow field by solving (38) in the initial flow domain:

$$\mathbf{F}_{\text{alg}}(\mathbf{T}^1, \mathbf{V}^1, \mathbf{P}^1; \mathbf{H}^0, \dot{\mathbf{H}}^0) = \mathbf{0}, \tag{44}$$

where the term $\dot{\mathbf{H}}^0$ is given by direct solution of (39). Initial values of $\mathbf{T}$ and $\mathbf{V}$ are used as first estimates in the Newton procedure. Steps (d) and (e) remain applicable.

The calculation of the flow field in (c) is by far the most costly operation in terms of computer time, for it involves the evaluation of an intricate Jacobian matrix and the solution of a large linear system. Fortunately, the use of predicted values as first estimates in the iterative process is so efficient that, in the simulations discussed hereafter, only one iteration has proven necessary to achieve full convergence. This strategy is much in the spirit of Gresho's technique for solving the Navier–Stokes equations in confined geometries (Gresho *et al.* [17]). We mention finally that automatic selection of the time increment can be made during the simulation, on the basis of the difference between predicted and corrected values and a user-specified level of local discretization errors. This capability has been exploited by Gresho *et al.* [17] and is readily available here as well. It is not used in the application reported below, however, where a constant time increment is chosen throughout the simulation.

Numerical Results

We have used the numerical procedure outlined above to simulate the growth of disturbances applied to a liquid jet issuing from a nozzle and leading eventually to breakup. The framework common to classical stability analyses is retained here: the actual spatial stability problem is formulated as a transient process in a frame of reference moving with the jet. In addition, the effects of the ambient medium are neglected and stresses generated prior to extrusion are assumed to be fully relaxed (see, e.g., Middleman [31]). We point out, however, that our analysis is not limited to small perturbations of the jet radius. In this context, we study the growth of a periodic disturbance applied to the radius of an infinitely long cylindrical jet. It is further assumed that the jet is axisymmetric at all times and that the wavelength of the disturbance remains constant during the growth. These hypotheses are well supported by experimental studies with externally controlled disturbances (see, e.g., Gordon *et al.* [15]).

In the present application, the integration domain Ω extends axially over half the wave length of the disturbance and the jet radius plays the role of the height function (Fig. 2). If δ denotes the dimensionless perturbation and h_0 the radius of the unperturbed liquid column, we have

$$h(z, t) = h_0[1 + \delta(z, t)]. \tag{45}$$

The primary goal of the present study is, given rheological parameters and initial conditions, to determine the function $\delta(z, t)$. In order to allow for a quantitative comparison between numerical results and linear stability analyses (referred to as LSA hereafter), we impose an initial perturbation of the form

$$\delta(z, 0) = \varepsilon \cos \frac{\pi}{L} z, \tag{46}$$

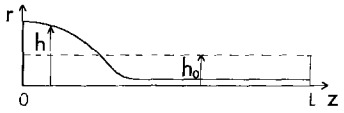

Fig. 2. Integration domain for the jet breakup problem; the flow is axisymmetric around the z-axis, and cylindrical coordinates are used.

where ε is a small parameter set here to 0.05. Similarly, we use the LSA results to specify the initial flow field (see the Appendix). The boundary conditions are:

(i) the stress condition (15) at the free surface,

(ii) symmetry conditions at $z=0$ (swell) and L (neck):

$$v_z = \frac{\partial v_r}{\partial z} = \frac{\partial h}{\partial z} = 0, \tag{47}$$

(iii) symmetry conditions at $r=0$:

$$v_r = \frac{\partial v_z}{\partial r} = 0. \tag{48}$$

For the sake of illustration, we have chosen a value of 20 for the dimensionless wavelength $2L/h_0$. Breakup will occur at the first occurrence of a vanishing value for the height function. In the finite element simulations, the numerical value for the breakup time is known within a fraction of the time increment, since the calculations are stopped when the predicted free surface meets the axis of the jet.

Three dimensionless groups arise in the present problem, namely a Reynolds number Re, a Deborah number De, and the ratio τ of characteristic times:

$$\mathrm{Re} = \rho\gamma h_0/6\mu^2, \qquad \mathrm{De} = \lambda_1\gamma/6\mu h_0, \qquad \tau = \lambda_2/\lambda_1. \tag{49}$$

The Deborah number is a measure of the viscoelastic character of the flow; it vanishes for a Newtonian fluid. The ratio τ is relevant only in the viscoelastic case. Lengths, times, velocities and stresses are made dimensionless by means of their respective characteristic values h_0, $6\mu h_0/\gamma$, $\gamma/6\mu$ and γ/h_0.

The present application provides a severe test for the numerical scheme. Indeed, the flow is driven only by capillary forces, which themselves are determined through the calculated free surface. As a first consequence, the stress condition (15) must be imposed accurately, which implies a rather refined discretization of the free surface and the neighboring flow field. Furthermore, we anticipate here the need for relatively small time increments to preserve the stability of the temporal integration.

It is not feasible to detail in this paper the wealth of information provided by the numerical technique. When presenting the results, we shall focus on the numerical output of primary relevance, namely the calculated free surface.

We first discuss the case of a Newtonian jet. Results of the simulation are depicted in Fig. 3 where we show the calculated flow domain and the finite element mesh at selected values of time. The Reynolds number is set here to 1.8, a value typical of experimental studies carried out by Goedde and Yuen [14] with aqueous glycerol solutions. The finite element mesh deforms according to (37); it involves 1458 nodal values for the velocity field, 205 for the pressure field and 81 for the height function, for a total of 1744 degrees of freedom. The time increment is 0.0025 and one time step is completed in 5.5 CPU seconds on an IBM 3081/K computer. Results indicate that the free surface keeps a cosinusoidal shape at the beginning of the process, in agreement with the LSA. This drastically changes from time $t = 8$ on, however, and breakup is predicted to occur away from the neck. We note the remarkable smoothness of the calculated free surface even when large variations of curvature occur just before breakup. Figure 3 agrees well with photographs presented by Goedde and Yuen [14]. It is indeed observed experimentally that the jet disintegrates into drops with ligaments between them; these ligaments form satellite drops if no post-merging with a main drop occurs. A detailed comparison with the LSA reveals the non-linear character of the jet dynamics. We give in Fig. 4 the amplitude of the perturbation as a function of time at both swell and neck, compared with the prediction of the LSA. Since the plot is semi-logarithmic, the latter is simply a straight line whose slope is the exponential growth rate α. Breakup times

analytical results at short times. This is indeed the case during the initial portion of the transient. The numerical results show, however, that non-linear behavior dominates the growth of the perturbation at later times. This is even more evident in Fig. 5 where we present the history of the jet radius at the axial position where breakup occurs. The jet radius first grows in agreement with the LSA until it reaches a maximum value at about $t = 8$. From that time on, it experiences a sud-

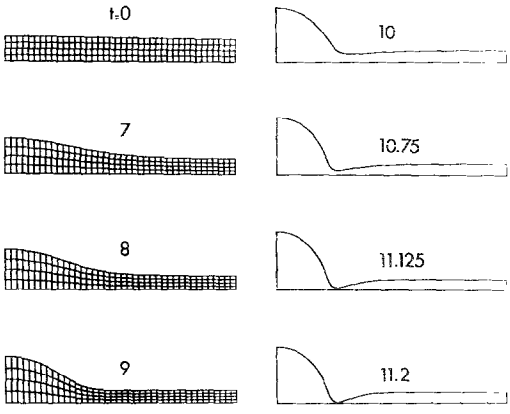

Fig. 3. Calculated flow domain and finite element grid at selected values of time; Newtonian fluid.

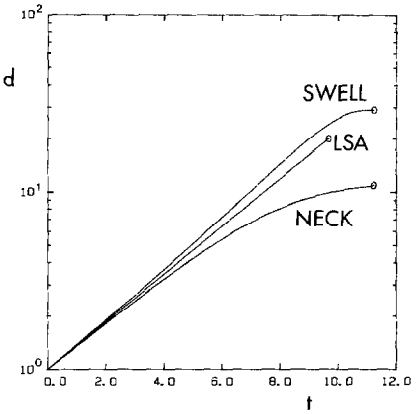

Fig. 4. Magnitude of the perturbation $d = |\delta|/\varepsilon$ as a function of time; Newtonian fluid; numerical results at swell ($z = 0$) and neck ($z = L$) and LSA prediction (see Appendix); the symbol 0 corresponds to breakup time.

den decrease leading to breakup. The presence of an inflection point at the very end of the curve has been confirmed by repeating the end of the simulation with a time increment equal to 0.001; however, this change of curvature might result from spatial discretization errors due to the extreme compression of the grid in the neighborhood of the breakup point.

Data brought together in Table I provide a more quantitative comparison between LSA and numerical results; in addition, significant indicators of the accuracy of the simulation are listed. We first give as a function of time the maximum difference $\Delta_{\mathrm{LSA,NUM}}$ between jet radii obtained from both analyses, relative to the initial radius h_0. Results agree very well at short times (for example, they differ only by 3% at time $t = 4$), but start deviating seriously after time $t = 7$

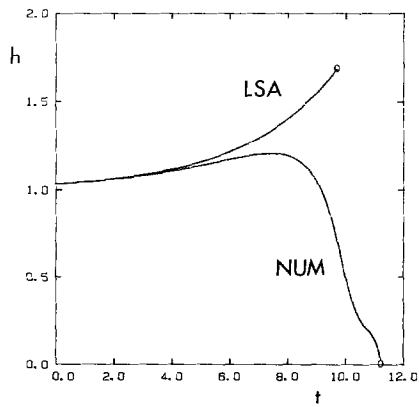

Fig. 5. History of the jet radius at the axial position where breakup is predicted numerically; Newtonian fluid; numerical and LSA predictions.

TABLE I

Characteristic Quantities for the Newtonian Jet

t	0.5	1	2	4	7	9	11.125	11.2
$\Delta_{\text{LSA.NUM}}$	8.10^{-4}	2.10^{-3}	5.10^{-3}	3.10^{-2}	2.10^{-1}	7.10^{-1}	—	—
$e_{\text{vol}}^{\text{NUM}}$	2.10^{-7}	4.10^{-7}	1.10^{-6}	5.10^{-6}	4.10^{-5}	1.10^{-4}	3.10^{-4}	3.10^{-4}
$e_{\text{vol}}^{\text{LSA}}$	5.10^{-4}	1.10^{-3}	3.10^{-3}	1.10^{-2}	1.10^{-1}	3.10^{-1}	—	—
e_h	3.10^{-8}	4.10^{-8}	6.10^{-8}	1.10^{-7}	3.10^{-7}	1.10^{-6}	8.10^{-6}	1.10^{-4}

because of non-linear effects. The incompressibility constraint ought to be satisfied accurately in the present application. It directly implies that the volume of fluid enclosed in the calculated flow domain should keep its initial value. We can thus obtain a measure of incompressibility errors generated during the simulation by means of the relative difference $e_{\text{vol}}^{\text{NUM}}$ between calculated and initial volumes. This quantity is given in Table I, as well as the corresponding difference $e_{\text{vol}}^{\text{LSA}}$ for the LSA results. One observes that the numerical scheme preserves mass remarkably well; indeed, the error is only 0.03% at the very last time step. The LSA, on the other hand, satisfies the incompressibility constraint only at first order in ε; as a result, it already suffers from a 10% error at time $t = 7$. It is worth noting that the LSA starts generating such inaccuracies precisely at the onset of non-linear effects predicted by the numerical technique.

Finally, the accuracy of the temporal integration can be assessed from the maximum difference e_h between predicted and corrected jet radii at each time step. This quantity is given in Table I relative to the predicted swell radius. We can safely conclude from inspection of these values that local time discretization errors are kept at a very low level throughout the integration.

Results for an Oldroyd–B fluid are presented in Fig. 6 for a Deborah number equal to 5 and a vanishing Reynolds number; we have selected a value of 0.25 for the ratio τ. The finite element grid contains 656 nodal variables for the elastic stress, 1134 for the velocity, 164 for the pressure and 81 for the jet radius, for a total of 2035 degrees of freedom. The time increment is 0.001 and one time step is completed in 9 CPU seconds.

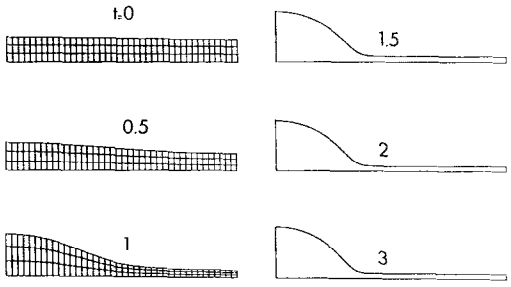

Fig. 6. Calculated flow domain and finite element grid at selected values of time; Oldroyd–B fluid.

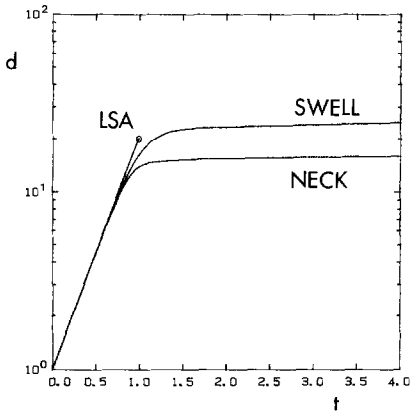

Fig. 7. Magnitude of the perturbation as a function of time; Oldroyd–B fluid; numerical results at swell and neck, and LSA predictions.

Our analysis predicts a cosinusoidal deformation of the free surface at short times, in close agreement with the LSA. From time $t = 1$ on, however, dramatic non-linear effects come into play: the growth rate of the perturbation suddenly decreases and the jet reaches a configuration of drops connected by filaments; these filaments keep on thinning, but at a much reduced speed. This is precisely what is observed experimentally with polymer solutions (see, e.g., Gordon *et al.* [15]). The simulation has been stopped at time $t = 4$ since the values of the radial velocity are then so small that they can hardly be discriminated from numerical noise.

Comparison with the LSA clearly demonstrates that the stabilizing character of elastic forces is the result of non-linear behavior. We show in Fig. 7 the growth of the perturbation at both swell and neck as obtained by the numerical scheme; the prediction of the LSA is again a straight line which ends in this case at time

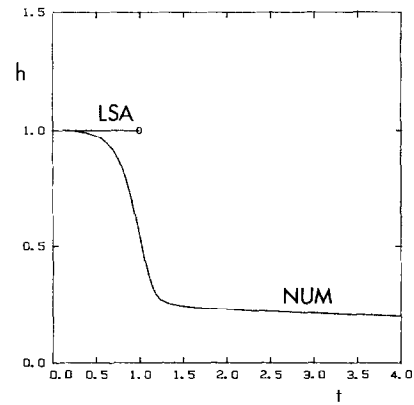

Fig. 8. History of the jet radius at the midpoint between neck and swell; Oldroyd–B fluid; numerical and LSA predictions.

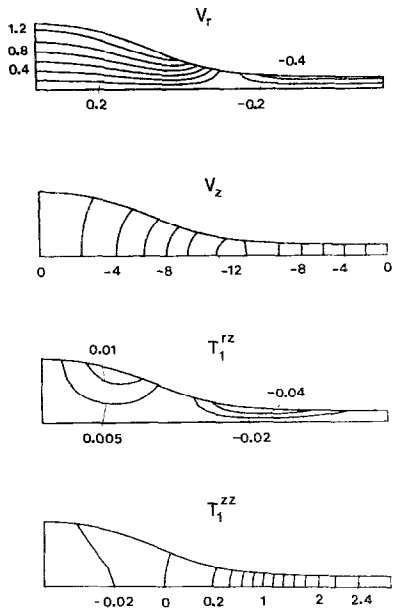

Fig. 9. Contour lines at time $t = 1$ for the velocity components v_r and v_z, and the elastic stress components T_1^{rz} and T_1^{zz}; Oldroyd-B fluid.

$t = 0.98$. Agreement between numerical and LSA results is remarkably good at short times, but a strong saturation effect is predicted numerically from time $t = 1$ on. The transition between the linear region, where the LSA is valid, and the slow stretching of the connecting filaments is very sharp. This is confirmed in Fig. 8, where we present the history of the jet radius at the midpoint between neck and swell; the LSA predicts a constant value for the radius there. A snapshot of the flow field in the non-linear regime is given in Fig. 9. The flow is practically elongational in the filament, which explains the large values for the elastic stress component T_1^{zz} there. The buildup of these elongational stresses during the growth of the disturbance is responsible for the stabilizing nature of elasticity.

Finally, we give in Table II the characteristic quantities defined previously during the discussion of Newtonian results. We can draw similar conclusions: (i) the

TABLE II

Characteristic Quantities for the Viscoelastic Jet

t	0.25	0.5	0.75	0.9	1	2	3	4
$\Delta_{LSA,NUM}$	4.10^{-3}	3.10^{-2}	1.10^{-1}	3.10^{-1}	—	—	—	—
e_{vol}^{NUM}	7.10^{-6}	5.10^{-5}	2.10^{-4}	3.10^{-4}	5.10^{-4}	7.10^{-4}	7.10^{-4}	7.10^{-4}
e_{vol}^{LSA}	5.10^{-3}	3.10^{-2}	1.10^{-1}	3.10^{-1}	—	—	—	—
e_h	9.10^{-7}	2.10^{-6}	3.10^{-6}	4.10^{-6}	3.10^{-6}	2.10^{-8}	1.10^{-8}	1.10^{-6}

agreement between numerical and LSA results is excellent at short times but deteriorates later on when non-linear behavior dominates; (ii) the incompressibility errors generated by the numerical scheme remain at a very low level throughout the simulation while the LSA presents inadmissible inaccuracies in that regard; (iii) the local discretization errors during the temporal integration are very small. It is interesting to note that the evolution of the quantity e_h reflects the different phases of the transient process.

Appendix

We summarize here the linear stability results used as initial conditions for the numerical simulations. Following the procedure described by Middleman [31], we have solved the dynamic problem obtained from linearization of both the governing equations (11–14) and the boundary condition (15). The non-linear terms present in the constitutive and momentum equations are neglected, and the linearized stress condition is applied at the unperturbed jet surface. All unknowns are sought in the complex form $f(r)e^{ikz+\alpha t}$, where k is the wave number of the perturbation ($k=\pi/L$), and α is the exponential growth rate. Application of the boundary conditions leads, after long developments, to a characteristic equation relating α to k. Middleman did not present the LSA results in their complete form, but rather he discussed an approximate formulation of the characteristic equation amenable to an analytical treatment. In the present paper, we use the exact formulation of the LSA results

$$\alpha^2+\frac{2\mu^* k^2}{\rho I_0(kh_0)}\left[I_1'(kh_0)-\frac{2kk'I_1(kh_0)I_1'(k'h_0)}{(k'^2+k^2)I_1(k'h_0)}\right]\alpha = \frac{\gamma k(1-k^2h_0^2)I_1(kh_0)(k'^2-k^2)}{\rho h_0^2(k'^2+k^2)I_0(kh_0)}, \tag{A1}$$

where

$$k'=\left(k^2+\frac{\alpha\rho}{\mu^*}\right)^{1/2}, \qquad \mu^*=\mu(1+\alpha\lambda_2)/(1+\alpha\lambda_1). \tag{A2}$$

Here, the symbol I_n denotes the modified Bessel function of the nth order. In the particular case of a Newtonian fluid, μ^* is equal to μ. We solve (A1) for the growth rate by means of a fixed point scheme, using the approximate result given by Middleman as a first guess. The characteristic equation (A1) has two solutions when the density is non-zero, which indicates that one can scale independently the initial perturbation of the jet radius and the initial flow field; we select here the solution corresponding to the highest growth rate.

The LSA solution then reads

$$
\begin{aligned}
h(z, t) &= h_0[1 + \varepsilon \cos kz\, e^{\alpha t}], \\
v_r(r, z, t) &= k[aI_1(kr) + bI_1(k'r)] \cos kz\, e^{\alpha t}, \\
v_z(r, z, t) &= -k\left[aI_0(kr) + b\left\{\frac{I_1(k'r)}{kr} + \frac{k'}{k} I_1'(k'r)\right\}\right] \sin kz\, e^{\alpha t}, \\
T_1^{rr}(r, z, t) &= 2ck[akI_1'(kr) + bk'I_1'(k'r)] \cos kz\, e^{\alpha t}, \\
T_1^{zz}(r, z, t) &= 2ck \cot kz\, v_z(r, z, t), \\
T_1^{\theta\theta}(r, z, t) &= 2cv_r(r, z, t)/r, \\
T_1^{rz}(r, z, t) &= -ck^2\left[2aI_1(kr) + bI_1(k'r)\frac{(k'^2 + k^2)}{k^2}\right] \sin kz\, e^{\alpha t},
\end{aligned}
\tag{A3}
$$

where ε is the small parameter used in (46), and a, b and c are constants given by

$$
\begin{aligned}
a &= -\frac{bI_1(k'h_0)(k'^2 + k^2)}{2k^2 I_1(kh_0)}, \\
b &= \frac{\varepsilon\alpha}{kI_1(k'h_0)[1 - ((k'^2 + k^2)/2k^2)]}, \\
c &= \mu^* - \mu\lambda_2/\lambda_1.
\end{aligned}
\tag{A4}
$$

The expressions (A3) written for time $t = 0$ provide the initial conditions used in the present paper. We note that only the initial velocity field is needed for a Newtonian fluid. The limiting case of a vanishing density is obtained by formal expansion of (A1)–(A4) around $\rho = 0$.

The nature of the LSA flow field is made more apparent by assuming that kr and $k'r$ are small and using classical asymptotic results for the Bessel functions; we find that $v_r \sim r \cos kz\, e^{\alpha t}$ and $v_z \sim \sin kz\, e^{\alpha t}$, which corresponds to a uniaxial stretching flow with a non-constant elongational rate.

ACKNOWLEDGMENTS

We gratefully acknowledge the Fellowship awarded to us by the Miller Institute for Basic Research in Science at the University of California, Berkeley. We also thank Professor Morton M. Denn for having suggested the study of jet breakup. His comments, as well as those received from Professor G. Marrucci at the early stage of this work, have been most valuable. Funds for numerical computation were made available through the Lawrence Berkeley Laboratory under programs supported by the Director, Office of Energy Research, Office of Basic Energy Sciences, Material Sciences Division of the U.S. Department of Energy, under Contract DE-AC03-76SF00098 and by the U.S. Army, ARRADCOM, under Agreement 3311-1412.

REFERENCES

1. R. B. BIRD, R. C. ARMSTRONG, AND O. HASSAGER, "Dynamics of Polymeric Liquids," Vol. 1, Wiley, New York, 1977.
2. D. B. BOGY, *Ann. Rev. Fluid Mech.* **11** (1979), 207.
3. R. BONNEROT AND P. JAMET, *J. Comput. Phys.* **25** (1977), 163.
4. D. W. BOUSFIELD, G. MARRUCCI, AND M. M. DENN, *in* "Advances in Rheology" (B. Mena *et al.*, Eds.), Vol. 2, p. 239, Elsevier, Amsterdam/New York, 1984.
5. R. M. CHRISTENSEN, "Theory of Viscoelasticity: An Introduction," Academic Press, New York/London, 1982.
6. M. J. CROCHET, A. R. DAVIES, AND K. WALTERS, "Numerical Simulation of Non-Newtonian Flow," Elsevier, New York, 1984.
7. M. J. CROCHET AND R. KEUNINGS, *J. Non-Newt. Fluid Mech.* **7** (1980), 199.
8. M. J. CROCHET AND R. KEUNINGS, *J. Non-Newt. Fluid Mech.* **10** (1982), 85.
9. M. J. CROCHET AND R. KEUNINGS, *J. Non-Newt. Fluid Mech.* **10** (1982), 339.
10. M. J. CROCHET AND R. KEUNINGS, *in* "Numerical Analysis of Forming Processes" (J. F. T. Pittman *et al.*, Eds.), Chap. 8, Wiley, New York, 1984.
11. M. J. CROCHET AND K. WALTERS, *Ann. Rev. Fluid Mech.* **15** (1983), 241.
12. B. A. FINLAYSON, *in* "Proceedings 5th Int. Symp. on Finite Elements and Flow Problems, Austin, Texas, 1984" (G. F. Carey and J. T. Oden, Eds.), p. 107.
13. C. S. FREDERIKSEN AND A. M. WATTS, *J. Comput. Phys.* **39** (1981), 282.
14. E. F. GOEDDE AND M. C. YUEN, *J. Fluid Mech.* **40** (1970), 495.
15. M. GORDON, J. YERUSHALMI, AND R. SHINNAR, *Trans. Soc. Rheol.* **17**:2 (1973), 303.
16. M. GOLDIN, J. YERUSHALMI, R. PFEFFER, AND R. SHINNAR, *J. Fluid Mech.* **38** (1969), 689.
17. P. M. GRESHO, R. L. LEE, AND R. L. SANI, *in* "Recent Advances in Numerical Methods in Fluids," Vol. 1, Pineridge Press, Swansea, U.K., 1980.
18. O. HASSAGER, *J. Non-Newt. Fluid Mech.* **9** (1981), 321.
19. O. HASSAGER AND C. BISGAARD, *J. Non-Newt. Fluid Mech.* **12** (1983), 153.
20. C. W. HIRT AND B. D. NICHOLS, *J. Comput. Phys.* **39** (1981), 201.
21. K. P. JACKSON, K. WALTERS, AND R. W. WILLIAMS, *J. Non-Newt. Fluid Mech.* **14** (1984), 173.
22. R. KEUNINGS, M. J. CROCHET, AND M. M. DENN, *Ind. Eng. Chem. Fundam.* **22** (1983), 347.
23. R. KEUNINGS AND M. J. CROCHET, *J. Non-Newt. Fluid Mech.* **14** (1984), 279.
24. R. KEUNINGS, *in* "Advances in Rheology" (B. Mena *et al.*, Eds.), Vol. 1, p. 699, Elsevier, Amsterdam/New York, 1984.
25. H. S. KHESHGI AND L. E. SCRIVEN, *in* "Finite Elements in Fluids" (R. H. Gallagher *et al.*, Eds.), Vol. 5, Wiley, New York, 1984.
26. S. J. LEE, M. M. DENN, M. J. CROCHET, A. B. METZNER, AND G. J. RIGGINS, *J. Non-Newt. Fluid Mech.* **14** (1984), 301.
27. V. G. LEVICH, "Physicochemical Hydrodynamics," Prentice-Hall, Englewood Cliffs, N.J., 1962.
28. D. R. LYNCH, *J. Comput. Phys.* **47** (1982), 387.
29. D. R. LYNCH AND W. G. GRAY, *J. Comput. Phys.* **36** (1980), 135.
30. M. J. MCCARTHY AND N. A. MOLLOY, *Chem. Eng. J.* **7** (1974), 1.
31. S. MIDDLEMAN, *Chem. Eng. Sci.* **20** (1965), 1037.
32. J. G. OLDROYD, *Proc. R. Soc. London Ser. A.* **200** (1950), 523.
33. K. J. RUSCHAK, *Int. J. Numer. Methods Eng.* **15** (1980), 639.
34. P. SCHUMMER AND K. H. TEBEL, *Ger. Chem. Eng.* **5** (1982), 209.
35. P. TOWNSEND, *J. Non-Newt. Fluid Mech.* **14** (1984), 265.
36. K. WALTERS, "Rheometry," Chapman & Hall, London, 1975.